Graphene-mediated stabilization of surface facets on metal substrates

Ganesh Ananthakrishnan, Mitisha Surana, Matthew Poss, et al.

View Online   Export Citation   CrossMark

ARTICLES YOU MAY BE INTERESTED IN

Graphene-mediated stabilization of surface facets on metal substrates

View Online   Export Citation   CrossMark

Ganesh Ananthakrishnan,[1,a)] 🆔 Mitisha Surana,[1] Matthew Poss,[2] Jad Jean Yaacoub,[2] Kaihao Zhang,[2]
Nikhil Admal,[2] Pascal Pochet,[3] 🆔 Sameh Tawfick,[2] 🆔 and Harley T. Johnson[1,2]

AFFILIATIONS

[1]Department of Materials Science and Engineering, University of Illinois at Urbana-Champaign, Urbana 61801, Illinois, USA
[2]Department of Mechanical Science and Engineering, University of Illinois at Urbana-Champaign, Urbana 61801, Illinois, USA
[3]Department of Physics, IriG, Univ. Grenoble-Alpes and CEA, Grenoble F-38054, France

[a)]Author to whom correspondence should be addressed: ganesha2@illinois.edu

ABSTRACT

After Chemical Vapor Deposition (CVD), faceted structures are routinely observed on a variety of metal catalyst surfaces in the graphene-covered regions. In spite of having its bare surface flattened through high diffusivity and surface pre-melting at high temperatures, the graphene-covered copper surface still presents faceted structures. Using atomistic simulations, we show the role of graphene in the preservation of the faceted surface morphology at the graphene–copper interface, manifesting as a suppressant against surface melting and surface-specific diffusion. The results of our molecular dynamics simulations are consistent with our experimental observations and demonstrate the thermo-mechanical interfacial surface stabilization role of graphene. Our study provides an understanding applicable to most metal–graphene interfaces and is especially relevant to most metallic catalysts for graphene growth by CVD. Understanding the interaction between graphene and the catalyst surface structure is critical for producing ultra-flat and defect-free graphene.

I. INTRODUCTION

Single and multi-layered graphene adsorbed on metal surfaces was first observed at least 50 years ago in preparation of platinum and ruthenium single crystal surfaces, during which carbon impurities were observed to segregate to the surface.[1–4] Such carbon on the surface radically affects properties of metals such as the catalytic and adsorptive activities, work functions, and the formation of fascinating features like Moiré structures on the metal surface.[5–7] In fact, the synthesis of graphene on metal catalyst substrates by chemical vapor deposition (CVD) results in the formation of a graphene–metal heterostructure, the properties of which strongly impact the functional performance of graphene.[8–20]

At high temperatures, the anisotropy of the surface free energy reduces and turns isotropic above the roughening transition temperature. This, coupled with the high atomic mobility at high temperatures, leads to the flattening of the surfaces as the metals reduce their surface area.[7,21–23] This explains the nominally flat surfaces seen on the bare metal at room temperatures after CVD growth.[24–27] Yet, faceted graphene–metal surfaces have been consistently observed on a wide variety of metal catalysts with different crystal orientations

and CVD growth conditions.[28–32] These facets contribute to nanoscale roughness, with features typically on the order of 20–100 nm step widths and heights. Faceting has been observed not only with graphene but also with hexagonal boron nitride systems.[33,34] In fact, faceted structures have been observed even when graphene flakes have been transferred onto the metal surface and annealed at high temperatures.[35] CVD temperatures for graphene growth on copper are generally close to the melting point of the metal, where the surface is reported to be pre-melted.[36,37] Despite this, faceted structures are observed only on the graphene-covered sites of the copper surface. A striking example is the observation of surface faceting when graphene is synthesized on molten copper at 1353K.[38] This can be seen in the magnified SEM images of hexagonal graphene flakes grown on liquid copper spheres shown in Fig. 1(b) of Ref. 38. This points to the critical role of graphene in locally controlling the phase of the substrate at its interface. This interfacial thermomechanical stabilization can be widely effective and critical in providing a complete explanation to experimentally observed surface faceting. Klaver *et al.*[39] demonstrated graphene-attributed melting suppression for two orientations of the copper surface, demonstrating increased

stability of graphene-covered surfaces relative to that of bare surfaces. The authors nevertheless argue that this melting suppression is not specific to surface orientation. However, the observation of faceted structures and their persistence under various synthesis conditions have motivated us to investigate the stability and orientation dependence of these faceted structures and surfaces in the copper-graphene system. The implications of this study extend to other metal–2D material interfaces where surface faceting is also observed.
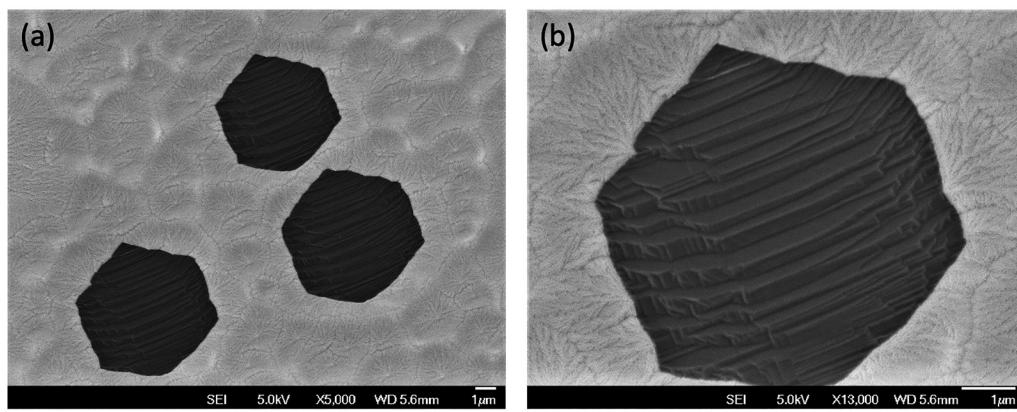
The work herein is motivated by Wang *et al.*, in which *in situ* environmental scanning electron microscope (ESEM) growth was used and demonstrated surface melting of the copper.[40] Our own experimental observations of copper surface melting during graphene growth are in good agreement. In the present work, we use molecular dynamics (MD) simulations in LAMMPS to corroborate graphene stabilization and preservation of surface faceted structures, which otherwise diffuse out given the high temperature for CVD synthesis. We relate this stabilization to the surface diffusivity of the metal catalysts at the interface with graphene. These results provide an important explanation for the preservation of surface step structures under graphene regardless of the details of the driving forces behind their formation.

II. EXPERIMENTAL OBSERVATIONS
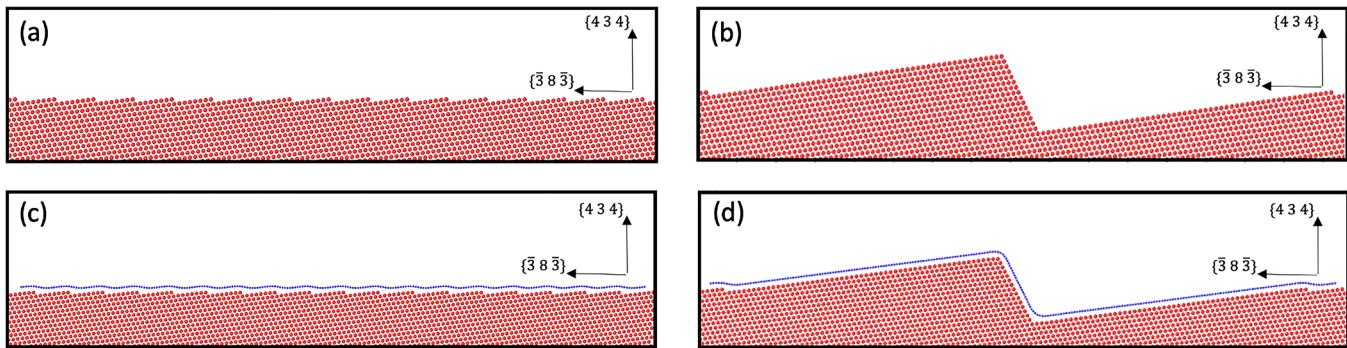
The CVD growth experiments performed in our study consistently show faceting, which indicates the transition from pre-melted surface to the solid surface associated with faceting of the graphene–metal interface. The reconstruction of metal surfaces during CVD at temperatures of 1000–1500 K is expected. For instance, using *in situ* environmental scanning electron microscopy (E-SEM), Wang *et al.* demonstrate copper surface pre-melting through their observation of oxide particle motion across the pre-melted copper surface.[40] However, during their *in situ* E-SEM experiment, the transition from the pre-melted surface to the solid surface with the faceted structures underneath graphene was not clearly observed. Our CVD growth experiments of graphene on copper clearly indicate this transformation in the postgrowth images.

For our experiments, acetone and IPA cleaned $25\,\mu$m copper foils were electropolished for 60 min at 1.9 V in 85% H_3PO_4 where another copper foil was used as a cathode. The foils were then washed with de-ionized (DI) water and IPA followed by annealing in the CVD furnace at 1000 °C, with a flow of helium and hydrogen gas (300 SCCM each) for 0.5 h, to remove other contaminants. This was followed by graphene growth using methane precursor gas (3 SCCM) in addition to the 300 SCCM flow of hydrogen and helium gases for 40 min. The growth was performed at atmospheric pressure and the sample was cooled to room temperature at 50 °C/min in helium. The sample was analyzed using a JEOL 7000F Scanning Electron Microscope (SEM). SEM images showed dendritic structures outside the graphene sites and a contrasting faceted copper structure under graphene as shown in Fig. 1. The considered graphene flakes all lie within the same copper grain, are always hexagonal, and are seen, consistently, with a faceted metal surface structure under the flakes.

Dendrite formation, seen in the regions surrounding the graphene flakes, has been reported by Langer and is the characteristic of solidification of the undercooled melt.[39,41] Our experiments were performed at temperatures near to, but below the nominal bulk melting temperature of copper, yet dendritic structures are nevertheless observed. This clearly indicates the existence of a pre-melted bare copper surface. In contrast, the surface under graphene is distinctly crystalline and faceted, pointing to an interfacial-thermomechanical stabilizing effect attributed to the presence of graphene. The faceted surface structures observed under the different flakes have similar facet widths, step densities, and similarly changing facet forms in different regions of the flake, implying similar surface orientations of the facets and a strong orientation dependence of the graphene–metal interface. The varying facet orientations on different grains further confirm the orientation dependence of this interface.[25,42] From these experimental observations, we hypothesize that graphene stabilizes the faceted surface structure and anisotropically modifies the surface diffusivity of the metal at high temperatures. In the present work, we use atomistic computational methods to probe this hypothesis.

FIG. 1. Scanning electron microscope images of graphene flakes on copper. (a) Three hexagonal flakes of graphene on the same grain showing faceted the copper structure in the graphene-covered regions and dendritic structures outside graphene. (b) Higher magnification image of one of the graphene flakes.

FIG. 2. (a) Perfect (4 3 4) surface with equidistant monatomic steps. (b) Step bunched structure with a height of 15 monatomic steps. (c) Perfect (4 3 4) surface covered with graphene. (d) Step bunched structure with a height of 15 monatomic steps covered with graphene.

III. COMPUTATIONAL METHODS

To study the effect of graphene on the faceted copper surface, we carry out molecular dynamics simulations of graphene flakes on copper surfaces of a thickness sufficient to approximate bulk-like behavior. The observed faceted structures themselves are expected to consist of low index and high symmetry surface orientations such as 111, 110, and 100. Indeed, these facets are observed commonly on surfaces that are not of high symmetry, via the formation of steps on the surface.[35] Surfaces oriented closely to high symmetry surfaces, or vicinal surfaces, are expected to transform to the respective high symmetry surfaces during the surface faceting transformation. These vicinal surfaces are made of flat terraces of the high symmetry orientation separated by atomic scale ledges or steps.[43] We choose for our calculations the (4 3 4) surface, which is vicinal to the (1 1 1) surface. All figures shown below are side views of the simulation box, enabling us to effectively observe the step structure progression with time.
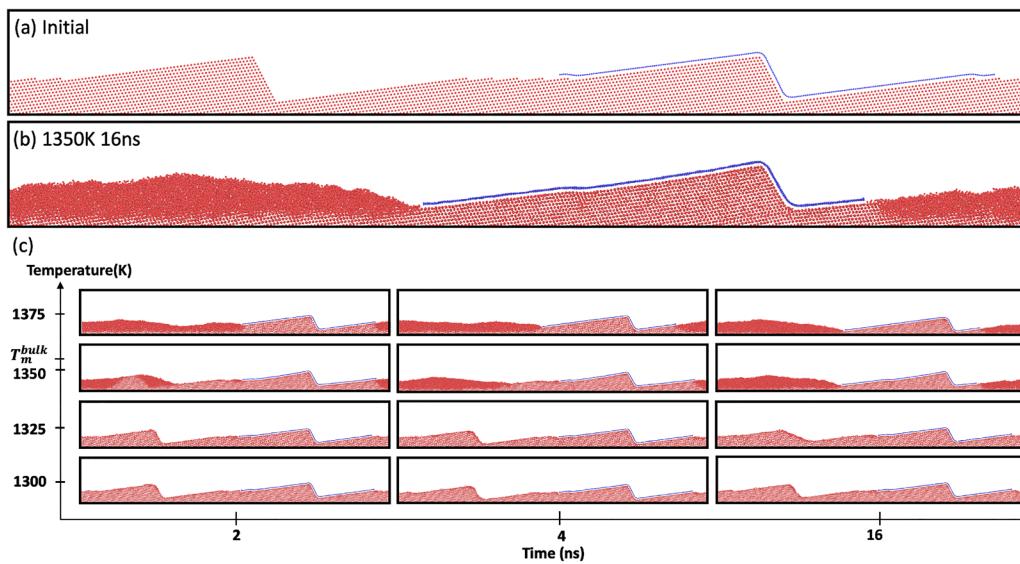
Figure 2(a) shows the (4 3 4) surface containing steps with single atomic height (monatomic) having a spacing of 16.5 Å with terraces of {1 1 1} type. This unit cell is periodic laterally and into the plane of the diagram. As part of a possible surface reconstruction, these monatomic steps may combine, or "bunch together," to form a faceted step structure like that in Fig. 2(b). In Fig. 2(b), the structure has facets of height 15 monatomic steps, constructed by rearranging atoms from the copper surface such that both surfaces of the faceted structure are of {1 1 1} type. The transformation from the (4 3 4) surface in Fig. 2(a) to the faceted structure shown in Fig. 2(b) is topologically feasible in our periodic supercell without any net addition or removal of atoms. The top-most point of the larger step structure and the bottom-most point of the structure shall be referred to as the "convex" and the "concave" edges, respectively. Figures 2(c) and 2(d) show the (4 3 4) surface and the larger step covered with graphene. The bends of graphene on the monatomic steps are referred to here as "monatomic bends" and the bends on the large step at the apex and at the bottom shall be called "convex" and "concave" bends, respectively.

We perform MD calculations using the Large scale Atomic/ Molecular Massively Parallel Simulator(LAMMPS).[44] We use a hybrid formulation of the empirical potentials, where the Cu–Cu,

C–C, and Cu–C interactions are modeled using Embedded-Atom Method (EAM), Adaptive Intermolecular Reactive Bond Order (AIREBO), and Lennard-Jones(L-J) potentials, respectively.[45,46] The Lennard-Jones (L-J) potential was parameterized in accordance with the simulations of Yi *et al.*[35] We use slab boundary conditions, with periodicity in all directions of the simulation box for all the simulations. The domain in the vertical (4 3 4) direction includes vacuum of 200 Å. The simulation box has a width of 33.5 Å in the (1 0 $\bar{1}$) direction perpendicular to the plane of the image. The length in the lateral direction ([$\bar{3}$ 8 $\bar{3}$]) of the simulation boxes of Figs. 3–5 is different and mentioned in the figure captions. The bottom layer of atoms of the copper slab with a thickness of 5 Å is frozen to mimic the bulk behavior of the atoms deeper into the surfaces. All MD calculations were visualized using the Open Visualization Tool (OVITO).[47] We perform an NVE dynamical simulation with Langevin thermostatting at a range of temperatures around the melting point of copper to investigate the effect of graphene on the melting of copper. As shown in Fig. 2, the simulation box includes a copper surface oriented in the (4 3 4) direction containing two large faceted step structures having surfaces of {1 1 1} type and a height of 15 monatomic steps. We further analyze the motion of the atoms on a (4 3 4) surface with two large steps having a height of 9 monatomic steps at 1250 K. For this calculation, we choose, for convenience, to track atoms at a depth of less than 12 Å from the (4 3 4) surface level. We have observed that the depth to which we consider atoms to be associated with the surface does not affect the trends of our results. We track their mean squared displacements (MSDs) in order to contrast the behavior between graphene-covered and bare copper atoms. The diffusivity of copper atoms can then be derived from the slope of the MSD with respect to time. The MSD calculations are only attempted for times greater than 5 ns into the simulation in order to obtain steady state values.

IV. MOLECULAR DYNAMICS RESULTS

We first present the MD simulation results at a range of temperatures around the bulk melting point to observe the effect of graphene on the melting of the copper surface. We then look more closely at the motion of the near-surface copper atoms at a given
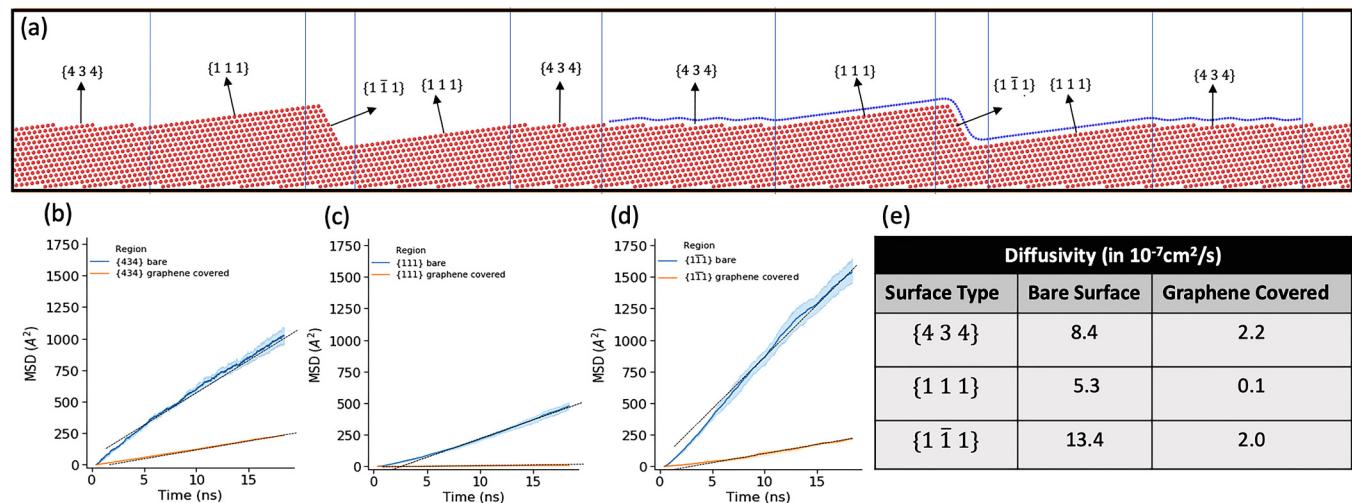
FIG. 3. Copper (4 3 4) surface partially covered with graphene containing two large steps (a) at the start of the simulation, (b) at 1350 K after 16 ns, and (c) in the form of a graphical map of snapshots on a temperature vs time plot. All images are projections through a three-dimensional structure that is approximately 33.5 Å in thickness so highly ordered regions show columns of atoms into the thickness, while disordered regions appear to have higher density. The simulation boxes for these calculations have a length of 659.1 Å in the lateral direction.

temperature to understand the role of mass transport on the surface stability.

In Fig. 3, we map out the partially graphene-covered copper surface profile from 0 to 16 ns at temperatures ranging from 1300 to 1375 K. The large uncovered faceted structure decomposes progressively at temperatures of 1300 and 1325 K. If we were to follow the dynamics for a longer time, we would expect the faceted structure to fully decompose into the flat (4 3 4) surface. This can also be seen with faceted structures of smaller height; in the Appendix, we show the results for a nine step facet. Although the

FIG. 4. Copper diffusivity on covered and uncovered surfaces having large facets of nine monatomic step height. (a) Supercell of the system with the demarcations separating dissimilar regions. Mean Squared Displacement (MSD) plots with respect to time showing 95% confidence intervals for graphene-covered and bare surface regions with orientations (b) (4 3 4), (c) (1 1 1), and (d) (1 $\bar{1}$ 1), and (e) table of diffusivities of all the regions. The simulation boxes for these calculations have a length of 560.2 Å in the lateral direction.

(1 1 1) surfaces of the larger 15 step faceted structure (shown in Fig. 3) have lower internal potential energy, the flat (4 3 4) surface with approximately equally spaced monatomic steps is entropically favorable. Hence, at temperatures sufficiently higher than the roughening transition point, the large step structure should transform into the flat (4 3 4) surface.[7,21–23,48] At temperatures of 1350 and 1375 K, the uncovered copper surface melts completely within a few nanoseconds. We observe surface melting on the bare surface of copper even at 1350 K, which is below the nominal melting temperature of bulk copper for the EAM potential.[45] This is in agreement with the literature and the observation of surface pre-melting by Wang *et al.*[40] Surface pre-melting is expected to be observed even at temperatures as low as 1100 K. However, this is not the case in our molecular dynamics calculations because of the limited time we can observe.[36,37]

At all temperatures shown in Fig. 3, the large graphene-covered faceted structures remain solid and mostly stable for the entire duration of the simulations. The entire structure covered by graphene remains solid for the duration of the simulation even at 1375 K, which is well above the nominal bulk melting temperature of the copper with this potential (T_m^{bulk}). Of course, melting may only be delayed, and it may occur only at times that are inaccessible using the present approach. Nevertheless, this shows that the graphene-covered copper surface is more stable than the bare surface, and in a small temperature window above the melting point, graphene stabilizes the solid preferentially over the liquid copper at the interface. The van der Waals bonding between graphene and the copper atoms close to the surface increases the cohesive energy of the graphene-covered copper surface, suppressing the melting of the surface.[49] In Fig. 3(b), the only indications of disorder in the graphene-covered region are seen at the convex and concave edges of the faceted structure as well as at the monatomic step. At these edges, graphene does not bind as strongly as the flat regions of the surface, as it needs to bend sharply to conform to the structure, suggesting that the stabilization of the surface depends on the quality of graphene-surface adherence. This would imply that flatter surfaces, such as high symmetry surfaces, are more stable under graphene cover as compared to other surface orientations.

To see the effects of graphene on the solid copper surface, we analyze the motion of near-surface atoms at temperatures further below the melting point. This is necessary to give perspective to the faceted structures observed on other metal substrates during CVD growth at temperatures below their bulk melting points. The MSD is a useful statistical tool to track the motion of atoms and to analyze the diffusivity of the copper atoms at the surface. In Figs. 4(b)–4(d), we see that the diffusivity of the graphene-covered copper atoms is significantly smaller than that of the bare surface copper atoms. This is true for all of the surfaces examined here and should extend to other surface orientations as well. The diffusivity values of the bare copper and graphene-covered copper calculated from our MD calculations lie between experimental values reported for surface diffusivity ($10^{-4} - 5 \times 10^{-4}$ cm^2/s) and bulk diffusivity ($2 \times 10^{-9} - 5 \times 10^{-9}$ cm^2/s).[50,51] The calculated diffusivity values become closer to the bulk diffusivity values as we take deeper depths of atoms from the (4 3 4) surface level into account.

On comparing the regions covered with graphene, there is an observably lower diffusivity on the (1 1 1) surface as compared to

the (4 3 4) or the (1 $\bar{1}$ 1) surface. This is due to the fact that graphene binds more strongly to the (1 1 1) surface as compared to other orientations. In the calculations, we have included the edges of the large faceted structure in the (1 $\bar{1}$ 1) region, which explains the difference in diffusivity compared to the (1 1 1) surface case. Graphene binds weakly to these edges causing the copper atoms there to be comparatively less stable and to contribute more to the diffusivity. Similarly, the (4 3 4) surface contains many monatomic steps at which graphene does not bind as strongly to the copper. The copper atoms at these monatomic step edges hence contribute to the greater diffusivity in these regions. Monatomic step edges and the large step edges are also sources for defects and act as mediators for diffusion. Thus, surfaces with fewer steps and edges, which are generally high symmetry low index surfaces, bind better to graphene and have more strongly suppressed surface diffusion. This can be observed through the higher 40-fold suppression of diffusion on the (1 1 1) surface as compared to the threefold suppression on the (4 3 4) surface. This preferential suppression of diffusion enables some diffusion on vicinal surfaces as compared to the stronger suppression on the low index surfaces. This, in turn, could aid the formation of larger high symmetry facets. In the bare copper surface regions, such a trend is not observed. The higher diffusivity observed on the bare (1 $\bar{1}$ 1) surface is due to the facet decomposition at the convex and concave edges of the large step, which are included in this region of the MSD calculation, as can be seen from Fig. 3.

V. DISCUSSION AND CONCLUSIONS

To investigate the stabilizing effects of graphene on the copper surface, we have probed the surface melting and surface diffusion effects of a graphene monolayer. Surface melting and surface diffusion are controlled by the interfacial bonding between graphene and copper. Graphene effectively passivates the under-coordinated copper atoms at the surface, thus increasing the cohesive energy of the latter. The increased cohesive energy locally raises the melting point of the copper surface,[49] thus stabilizing the surface against melting and equivalently lowering the mobility of the atoms at the surface. We have also seen from our calculations that the surface diffusion suppression is orientation specific. This stems from the weaker bonding between graphene and low symmetry surfaces containing steps, where graphene is less conformal to the stepped surface. The weaker bonding directly implies the weaker cohesive energy of the copper atoms at these step edges, which, in turn, are more mobile and contribute to the diffusivity.

The physics behind this effect can be generalized to any material that does not exhibit a self-passivating surface reconstruction, as is common in semiconductor surfaces.[52,53] This will be the case, in particular, for metallic surfaces that do not have such an *intrinsic* surface passivation mechanism. For these metallic systems, graphene will act as an *extrinsic* passivation layer leading to the suppression of surface diffusion and surface melting at the metal–graphene interface. The same mechanism is also expected to be applicable to metallic nanowires inside carbon nanotubes (CNTs) or metallic clusters caged in carbon fullerenes. This highlights the key role of one-atom-thick carbon layers to boost the thermal stability of different types of materials.

This stabilization of a solid metal phase at a carbon interface can explain some of the effects seen in studies of wetting of single walled carbon nanotubes (SWCNTs) with metals.[54] Specifically, the melting point of metal nanowires encapsulated in CNTs can be significantly higher than in the bulk, although bare metal nanowires have a lower melting point than the bulk. This creates useful opportunities for the use of such small nanowires encapsulated in CNTs, where the CNT shells effectively passivate the metal surfaces,[55] opening opportunities in devices ranging from batteries to nanocomposites. Second, the barrier to diffusion can explain the difficulty in filling small CNTs with molten metals, which has previously only been attributed to wetting and affinity between the carbon nanomaterials and the filling medium.[56,57] Indeed, recent work by Fang *et al.* shows anomalous melting transition behavior of aluminum nanowires encapsulated in SWCNTs of certain radii. Atoms from the inner layers of the aluminum nanowire diffuse to the surface, forming a metal shell of few layers bound to the inner wall of the SWCNT. This metal shell later melts at a temperature higher than the bulk melting point.[58] Based on the results of our study, we postulate that this might be a direct result of the suppressed melting at the graphene–metal interface leading to the prior melting of the bulk inner layers of the aluminum nanowire, which consequently diffuse to the interface and form the solid shell. The higher melting point of the metal shell atoms bound to the inner wall of the SWCNT is due to their increased cohesive energy caused by the van der Waals bonding. Other theoretical studies have also shown the melting of inner layers prior to the outer layers of the nanowire when encapsulated in CNTs.[59]

Another useful consequence of this interfacial interaction is that dewetting of metallic, polymer, and organic semiconductor thin films is completely eliminated by covering the film surface with graphene or other 2D materials. Cao *et al.* attribute this to the surface stabilization effect of the 2D materials involving the suppression of surface fluctuations.[60] Dewetting of metallic thin films occurs through a surface diffusion mechanism.[61] Hence, the graphene-based suppression of surface diffusion is expected to have a major contribution to the elimination of dewetting. Cao *et al.* attribute reduced susceptibility to dewetting to better adherence of the 2D material to the surface.[60] This may also be directly related to our observation of orientation dependent suppression of diffusivity, where surfaces with steps having imperfect adherence to graphene exhibit more surface diffusivity. The understanding of these high temperature effects at graphene–metal interfaces should be considered in engineering graphene and other 2D materials into new devices.

In summary, we demonstrate the role of graphene on the high temperature stability of the graphene–metal interface. This stabilization has been demonstrated using MD simulations, which are compared to experimental observations. Both show that surface melting is achieved at lower temperatures—or at shorter exposure to high temperatures—on bare copper as compared to a faceted graphene-covered metal surface. At lower temperatures, graphene suppresses diffusion on the metal surface. The suppression of diffusion is more effective on flat, high symmetry surfaces where graphene attaches more conformally to the surface. This preferential suppression of diffusion on low index planes contributes to the stability of faceted structures observed in heated graphene–metal interfaces.
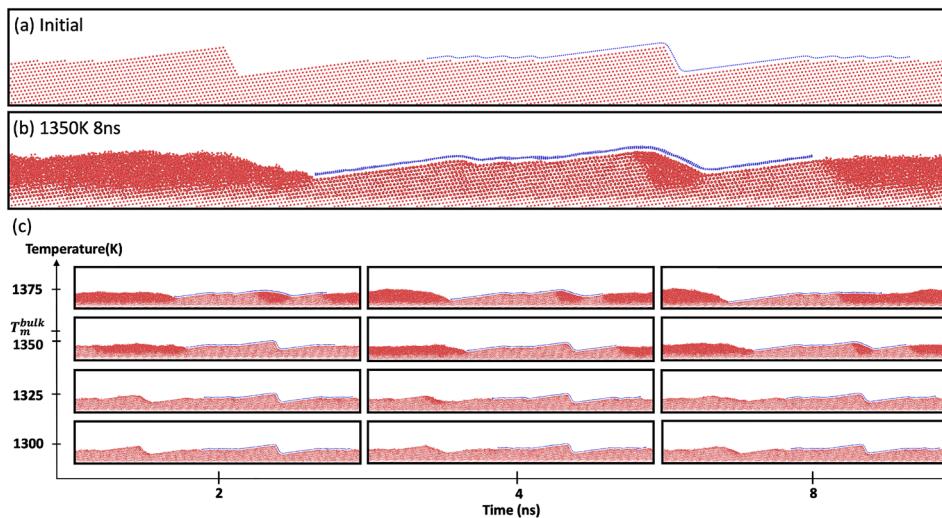
APPENDIX: SURFACE MELTING FOR NINE STEP FACET

In Fig. 5, we map out the dynamics of the partially graphene-covered copper surface with nine step facets from 0 to 8 ns at temperatures ranging from 1300 to 1375 K.

The uncovered copper surface starts melting prior to 2 ns of the simulation, similar to the 15 step facet case analyzed in the main text.

FIG. 5. Copper (4 3 4) surface partially covered with graphene containing two large steps (a) at the start of the simulation, (b) at 1350 K after 8 ns, and (c) in the form of a graphical map of snapshots on a temperature vs time plot. All images are projections through a three-dimensional structure that is approximately 33.5 Å in thickness, so highly ordered regions show columns of atoms into the thickness, while disordered regions appear to have higher density. The simulation boxes for these calculations have a length of 560.2 Å in the lateral direction.

Concurrently, we see a faster destructuring of the uncovered nine step facet toward the flat {4 4 3} surface at 1325 and 1300 K, respectively. This further supports the hypothesis that the uncovered faceted surface tends toward the flat configuration mentioned in the main text. At 1350 K, the graphene-covered nine step facet starts melting after 4 ns and is molten at 8 ns whereas at 1375 K melting occurs earlier than 2 ns. This also suggests that the melting of the graphene-covered copper surface might just be delayed in the 15 step facet case. Melting under the graphene nucleates at the concave and convex step edges of the nine step facet, which are susceptible to high energy sites and in close proximity to each other.

DATA AVAILABILITY

The data that support the findings of this study are available within the article.

REFERENCES

[1]S. Hagstrom, H. B. Lyon, and G. A. Somorjai, Phys. Rev. Lett. **15**, 491 (1965).
[2]A. E. Morgan and G. A. Somorjai, Surf. Sci. **12**, 405 (1968).
[3]J. T. Grant and T. W. Haas, Surf. Sci. **21**, 76 (1970).
[4]J. W. May, Surf. Sci. **17**, 267 (1969).
[5]J. Wintterlin and M. L. Bocquet, Surf. Sci. **603**, 1841 (2009).
[6]A. Y. Tontegode, Prog. Surf. Sci. **38**, 201 (1991).
[7]J. M. Blakely and C. C. Umbach, in *Diffusion at Interfaces: Microscopic Concepts*, edited by M. Grunze, J. J. Weimer, and H. J. Kreuzer (Springer, Berlin, 1988), pp. 102–110.
[8]X. Li, W. Cai, J. An, S. Kim, J. Nah, D. Yang, R. Piner, A. Velamakanni, I. Jung, E. Tutuc, S. K. Banerjee, L. Colombo, and R. S. Ruoff, Science **324**, 1312 (2009).
[9]Y. Hao, M. S. Bharathi, L. Wang, Y. Liu, H. Chen, S. Nie, X. Wang, H. Chou, C. Tan, B. Fallahazad, H. Ramanarayan, C. W. Magnuson, E. Tutuc, B. I. Yakobson, K. F. McCarty, Y. W. Zhang, P. Kim, J. Hone, L. Colombo, and R. S. Ruoff, Science **342**, 720 (2013).
[10]X. Xu, Z. Zhang, L. Qiu, J. Zhuang, L. Zhang, H. Wang, C. Liao, H. Song, R. Qiao, P. Gao, Z. Hu, L. Liao, Z. Liao, D. Yu, E. Wang, F. Ding, H. Peng, and K. Liu, Nat. Nanotechnol. **11**, 930 (2016).
[11]A. Reina, X. Jia, J. Ho, D. Nezich, H. Son, V. Bulovic, M. S. Dresselhaus, and K. Jing, Nano Lett. **9**, 30 (2009).
[12]K. S. Kim, Y. Zhao, H. Jang, S. Y. Lee, J. M. Kim, K. S. Kim, J. H. Ahn, P. Kim, J. Y. Choi, and B. H. Hong, Nature **457**, 706 (2009).
[13]T. Gao, S. Xie, Y. Gao, M. Liu, Y. Chen, Y. Zhang, and Z. Liu, ACS Nano **5**, 9194 (2011).
[14]L. Gao, W. Ren, H. Xu, L. Jin, Z. Wang, T. Ma, L. P. Ma, Z. Zhang, Q. Fu, L. M. Peng, X. Bao, and H. M. Cheng, Nat. Commun. **3**, 699 (2012).
[15]Z. J. Wang, J. Dong, Y. Cui, G. Eres, O. Timpe, Q. Fu, F. Ding, R. Schloegl, and M. G. Willinger, Nat. Commun. **7**, 1 (2016).
[16]P. W. Sutter, J. I. Flege, and E. A. Sutter, Nat. Mater. **7**, 406 (2008).
[17]Y. Pan, H. Zhang, D. Shi, J. Sun, S. Du, F. Liu, and H. J. Gao, Adv. Mater. **21**, 2777 (2009).
[18]S. Roth, J. Osterwalder, and T. Greber, Surf. Sci. **605**, L17 (2011).
[19]M. Sicot, S. Bouvron, O. Zander, U. Rüdiger, Y. S. Dedkov, and M. Fonin, Appl. Phys. Lett. **96**, 093115 (2010).
[20]N. Blanc, F. Jean, A. V. Krasheninnikov, G. Renaud, and J. Coraux, Phys. Rev. Lett. **111**, 1 (2013).
[21]W. W. Mullins, Interface Sci. **9**, 9 (2001).
[22]H.-N. Yang, T.-M. Lu, and G.-C. Wang, Phys. Rev. Lett. **63**, 1621 (1989).
[23]J. Lapujoulade and B. Salanon, "The roughening transition on surfaces," in *Phase Transitions in Surface Films 2* (Springer US, Boston, MA, 1991) pp. 217–246.
[24]X. H. Kong, H. X. Ji, R. D. Piner, H. F. Li, C. W. Magnuson, C. Tan, A. Ismach, H. Chou, and R. S. Ruoff, Appl. Phys. Lett. **103**, 043119 (2013).
[25]J. H. Kang, J. Moon, D. J. Kim, Y. Kim, I. Jo, C. Jeon, J. Lee, and B. H. Hong, Nano Lett. **16**, 5993 (2016).
[26]J. S. Yu, X. Jin, J. Park, D. H. Kim, D. H. Ha, D. H. Chae, W. S. Kim, C. Hwang, and J. H. Kim, Carbon **76**, 113 (2014).
[27]D. Luo, X. You, B. W. Li, X. Chen, H. J. Park, M. Jung, T. Y. Ko, K. Wong, M. Yousaf, X. Chen, M. Huang, S. H. Lee, Z. Lee, H. J. Shin, S. Ryu, S. K. Kwak, N. Park, R. R. Bacsa, W. Bacsa, and R. S. Ruoff, Chem. Mater. **29**, 4546 (2017).
[28]M. S. Bronsgeest, N. Bendiab, S. Mathur, A. Kimouche, H. T. Johnson, J. Coraux, and P. Pochet, Nano Lett. **15**, 5098 (2015).
[29]M. Huang, M. Biswal, H. J. Park, S. Jin, D. Qu, S. Hong, Z. Zhu, L. Qiu, D. Luo, X. Liu, Z. Yang, Z. Liu, Y. Huang, H. Lim, W. J. Yoo, F. Ding, Y. Wang, Z. Lee, and R. S. Ruoff, ACS Nano **12**, 6117 (2018).
[30]E. Rokuta, Y. Hasegawa, A. Itoh, K. Yamashita, T. Tanaka, S. Otani, and C. Oshima, Surf. Sci. **427–428**, 97 (1999).
[31]T. Fujita, W. Kobayashi, and C. Oshima, Surf. Interface Anal. **37**, 120 (2005).
[32]Y. Shi, A. A. Zakharov, I. G. Ivanov, G. R. Yazdi, V. Jokubavicius, M. Syväjärvi, R. Yakimova, and J. Sun, Carbon **140**, 533 (2018).
[33]L. Wang, X. Xu, L. Zhang, R. Qiao, M. Wu, Z. Wang, S. Zhang, J. Liang, Z. Zhang, Z. Zhang, W. Chen, X. Xie, J. Zong, Y. Shan, Y. Guo, M. Willinger, H. Wu, Q. Li, W. Wang, P. Gao, S. Wu, Y. Zhang, Y. Jiang, D. Yu, E. Wang, X. Bai, Z. J. Wang, F. Ding, and K. Liu, Nature **570**, 91 (2019).
[34]L. Liu, J. Park, D. A. Siegel, K. F. McCarty, K. W. Clark, W. Deng, L. Basile, J. C. Idrobo, A.-P. Li, and G. Gu, Science **343**, 163 (2014).
[35]D. Yi, D. Luo, Z.-J. Wang, J. Dong, X. Zhang, M.-G. Willinger, R. S. Ruoff, and F. Ding, Phys. Rev. Lett. **120**, 246101 (2018).
[36]B. Chatterjee, Nature **275**, 203 (1978).
[37]J. W. Frenken and J. F. Van Der Veen, Phys. Rev. Lett. **54**, 134 (1985).
[38]D. Geng, B. Wu, Y. Guo, L. Huang, Y. Xue, J. Chen, G. Yu, L. Jiang, W. Hu, and Y. Liu, Proc. Natl. Acad. Sci. U.S.A. **109**, 7992 (2012).
[39]T. P. C. Klaver, S.-E. Zhu, M. H. F. Sluiter, and G. Janssen, Carbon **82**, 538 (2015).
[40]Z. J. Wang, G. Weinberg, Q. Zhang, T. Lunkenbein, A. Klein-Hoffmann, M. Kurnatowska, M. Plodinec, Q. Li, L. Chi, R. Schloegl, and M. G. Willinger, ACS Nano **9**, 1506 (2015).
[41]J. S. Langer, Rev. Mod. Phys. **52**, 1 (1980).
[42]K. Hayashi, S. Sato, and N. Yokoyama, Nanotechnology **24**, 025603 (2013).
[43]V. B. Shenoy and L. B. Freund, J. Mech. Phys. Solids **50**, 1817 (2002).
[44]S. Plimpton, "Fast parallel algorithms for short-range molecular dynamics," J. Comput. Phys. **117**, 1–19 (1995).
[45]M. I. Mendelev, M. J. Kramer, C. A. Becker, and M. Asta, Philosophical Magazine **88**, 1723 (2008).
[46]S. J. Stuart, A. B. Tutein, and J. A. Harrison, J. Chem. Phys. **112**, 6472 (2000).
[47]A. Stukowski, Modell. Simul. Mater. Sci. Eng. **18**, 015012 (2010).
[48]N. Akutsu and T. Yamamoto, *Handbook of Crystal Growth*, 2nd ed. (Elsevier, 2015), Vol. 1, pp. 265–313.
[49]K. K. Nanda, S. N. Sahu, and S. N. Behera, Phys. Rev. A: At., Mol., Opt. Phys. **66**, 132081 (2002).
[50]H. P. Bonzel and N. A. Gjostein, Phys. Status Solidi B **25**, 209 (1968).
[51]J. Kučera and B. Million, Metall. Trans. **1**, 2599 (1970).
[52]C. B. Duke, Chem. Rev. **96**, 1237 (1996).
[53]H. Shinohara, Rep. Prog. Phys. **64**, 297 (2001).
[54]P. M. Ajayan and S. Lijima, Nature **361**, 333 (1993).
[55]Y. Wu and P. Yang, Appl. Phys. Lett. **77**, 43 (2000).
[56]D. Ugarte, A. Châtelain, and W. A. De Heer, Science **274**, 1897 (1996).
[57]E. Dujardin, T. W. Ebbesen, H. Hiura, and K. Tanigaki, Science **265**, 1850 (1994).
[58]R. R. Fang, Y. Z. He, K. Zhang, and H. Li, J. Phys. Chem. C **118**, 7622 (2014).
[59]J. Shao, C. Yang, X. Zhu, and X. Lu, J. Phys. Chem. C **114**, 2896 (2010).
[60]P. Cao, P. Bai, A. A. Omrani, Y. Xiao, K. L. Meaker, H. Z. Tsai, A. Yan, H. S. Jung, R. Khajeh, G. F. Rodgers, Y. Kim, A. S. Aikawa, M. A. Kolaczkowski, Y. Liu, A. Zettl, K. Xu, M. F. Crommie, and T. Xu, Adv. Mater. **29**, 1 (2017).
[61]C. V. Thompson, Annu. Rev. Mater. Res. **42**, 399 (2012).